

Table S1 The RegCM4 model configuration used in this study.

Contents	Description
Domain	50-km horizontal resolution; Central lat. and lon.: 35° N, 115° E; 200 (lon.) × 130 (lat.)
Vertical layers (top)	18 vertical sigma levels (1 hPa)
PBL scheme	Holtslag
Cumulus parameterization scheme	Emanuel
Land surface model	NCAR CLM3.5
Short-/longwave radiation scheme	NCAR CCM3
Boundary data	ERA-Interim (ERA); MPI-ESM-MR (MPI)
Climate scenario	RCP4.5; RCP8.5
Simulation period	Jan. 1970–Dec. 2000; Jan. 2020–Dec. 2050
Analysis period	Jan. 1971–Dec. 2000; Jan. 2021–Dec. 2050

Table S2 The KS test statistics and AIC values for the extreme precipitation indices under different distributions.

Index	KS value				AIC				Best distribution
	Gumbel	GAMMA	Ex	GEV	Gumbel	GAMMA	Ex	GEV	
PRCPTOT	0.27	0.13	0.60	0.27	290.2	285.6	403.6	287.3	GAMMA
SDII	0.17	0.23	0.47	0.23	9.2	1.1	141.1	3.2	GAMMA
RX1day	0.07	0.10	0.57	0.13	133.9	136.3	248.9	133.5	GEV
RX5day	0.13	0.17	0.47	0.10	173.2	172.3	278.4	171.5	GEV
R95	0.13	0.17	0.47	0.13	244.4	240.9	318.5	238.6	GEV
R99	0.13	0.23	0.50	0.13	199.1	200.0	251.6	198.6	GEV
CDD	0.13	0.13	0.53	0.13	190.8	187.1	311.1	188.6	GAMMA
CWD	0.17	0.17	0.47	0.17	54.5	50.9	174.8	52.1	GAMMA
R0.1	0.23	0.13	0.73	0.13	194.3	189.3	355.9	190.2	GAMMA

The bold front indicates that the distribution did not pass the 0.95 confidence level.

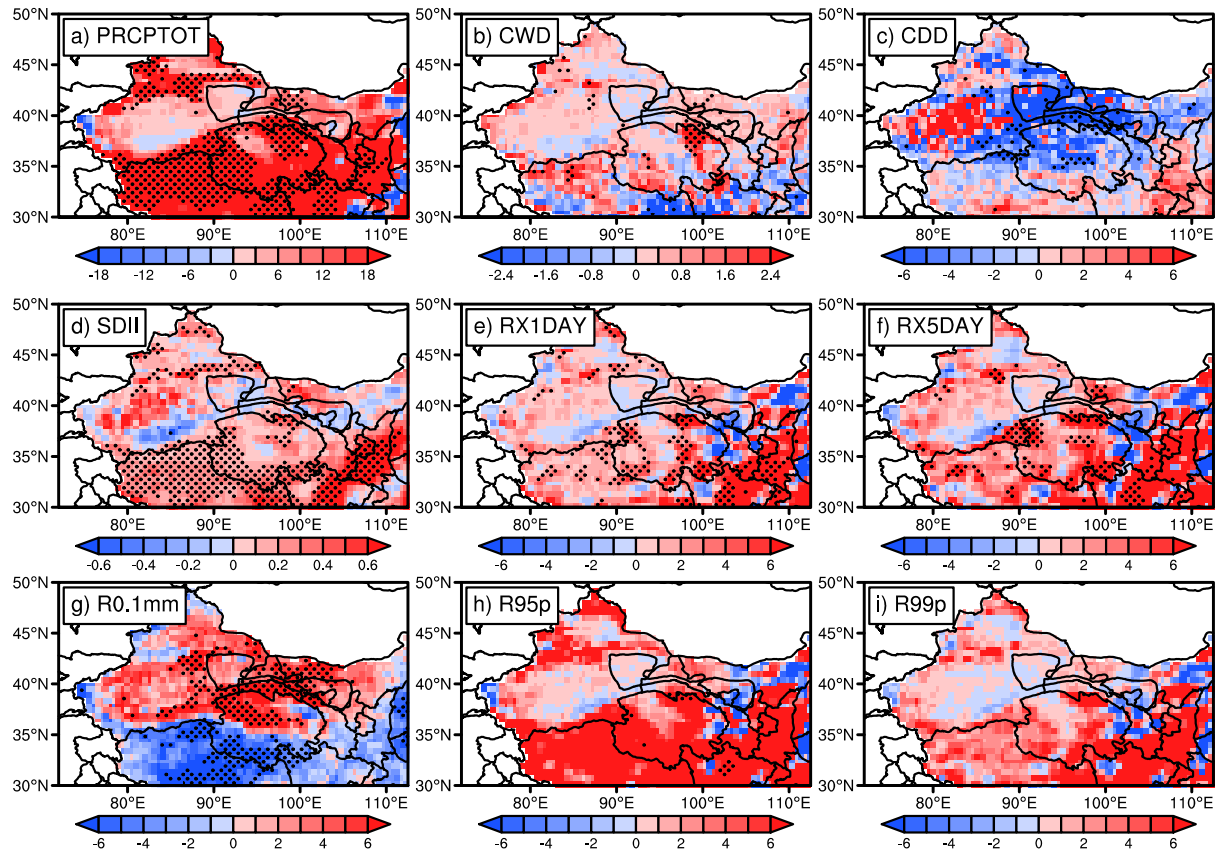


Figure S1. Multiyear average changes of extreme precipitation indices under the RCP4.5 compared to the reference period. The black dots represent statistically significant differences at the 95% significance level based on Student's t-test.

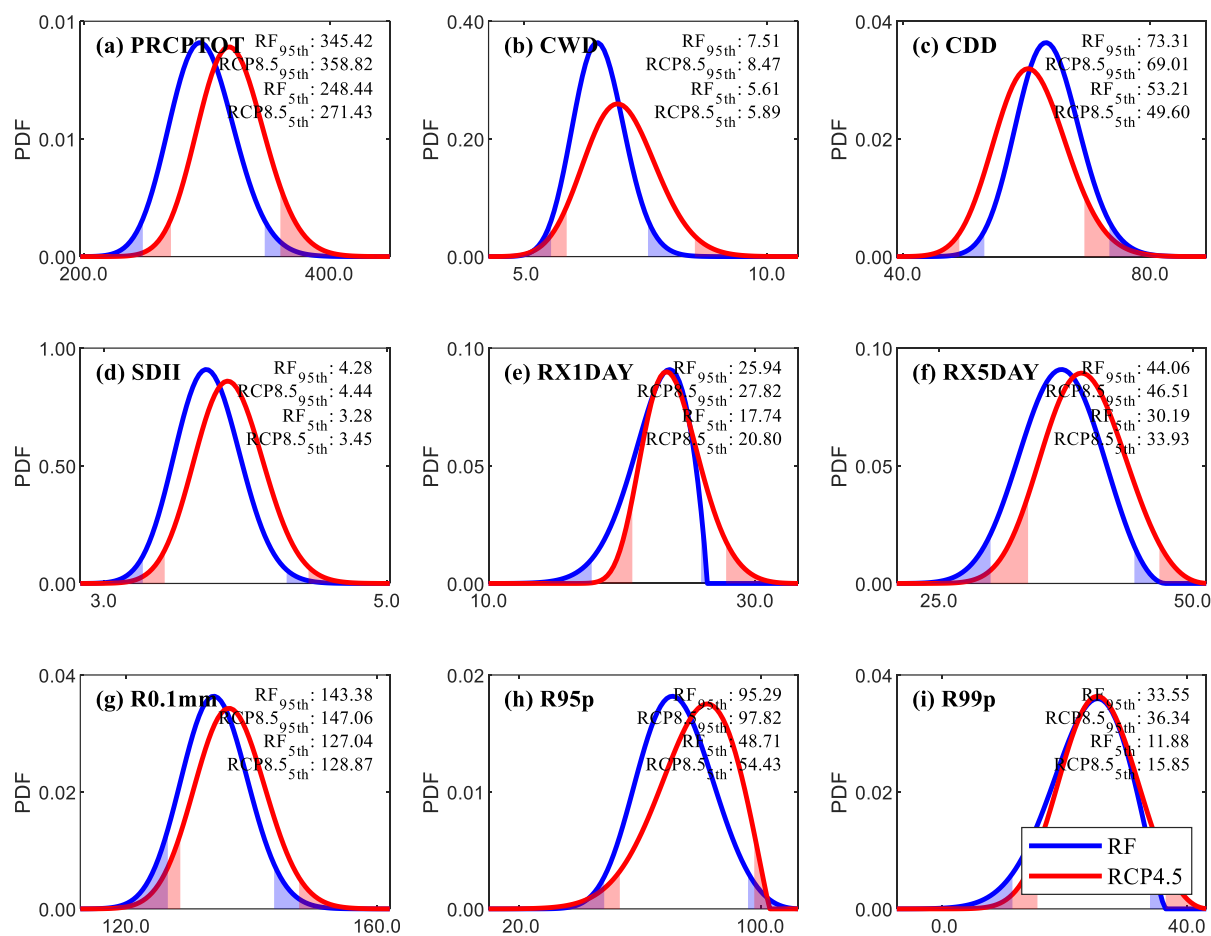


Figure S2. Annual probability density function (PDF) of Northwest China averaged extreme precipitation indices from 1971 to 2000 (blue line, RF) and from 2021 to 2050 (red line, RCP4.5)—consideration of portions exceeding the 95th percentile and below the 5th percentile.

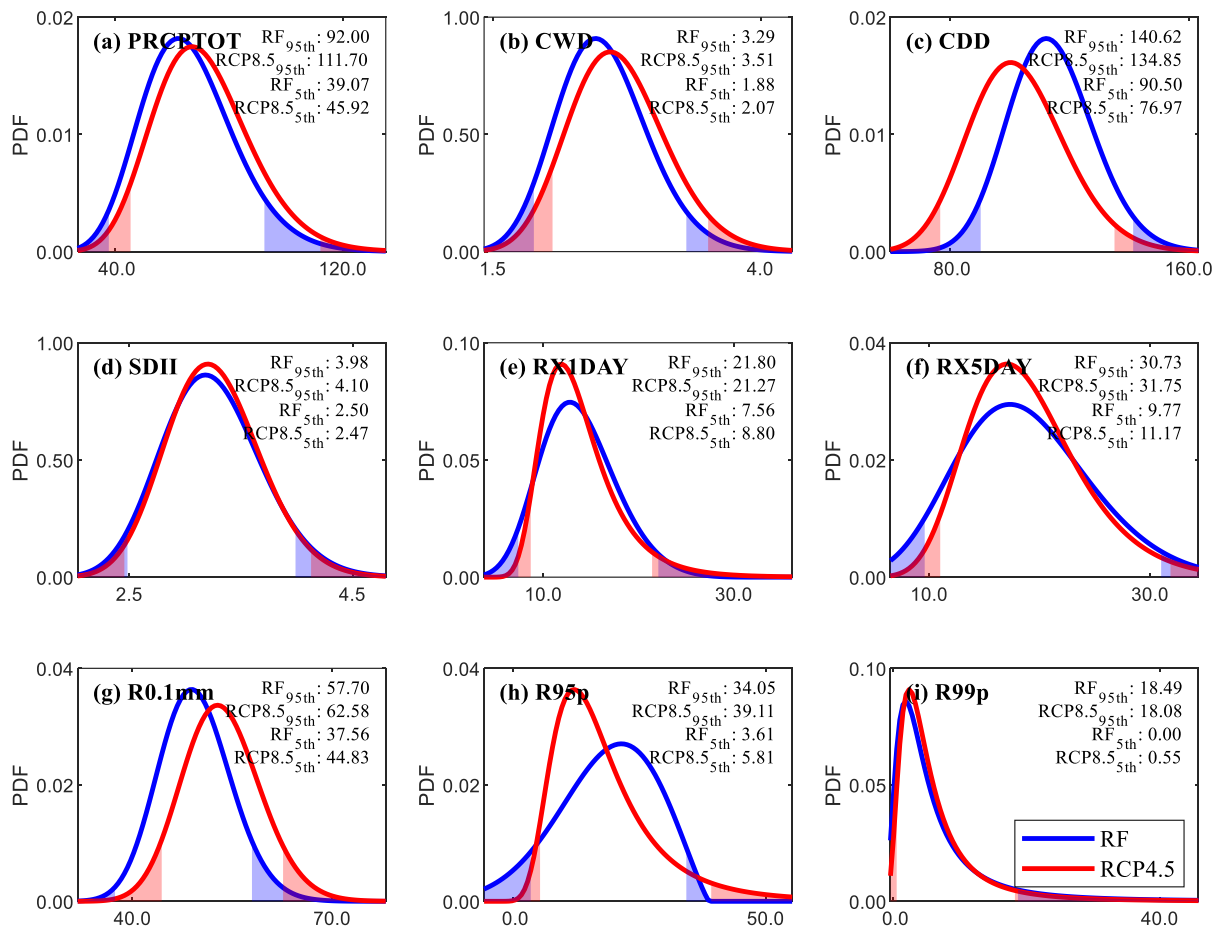


Figure S3. Annual probability density function (PDF) of the irrigation district averaged extreme precipitation indices from 1971 to 2000 (blue line, RF) and from 2021 to 2050 (red line, RCP4.5)—consideration of portions exceeding the 95th percentile and below the 5th percentile.

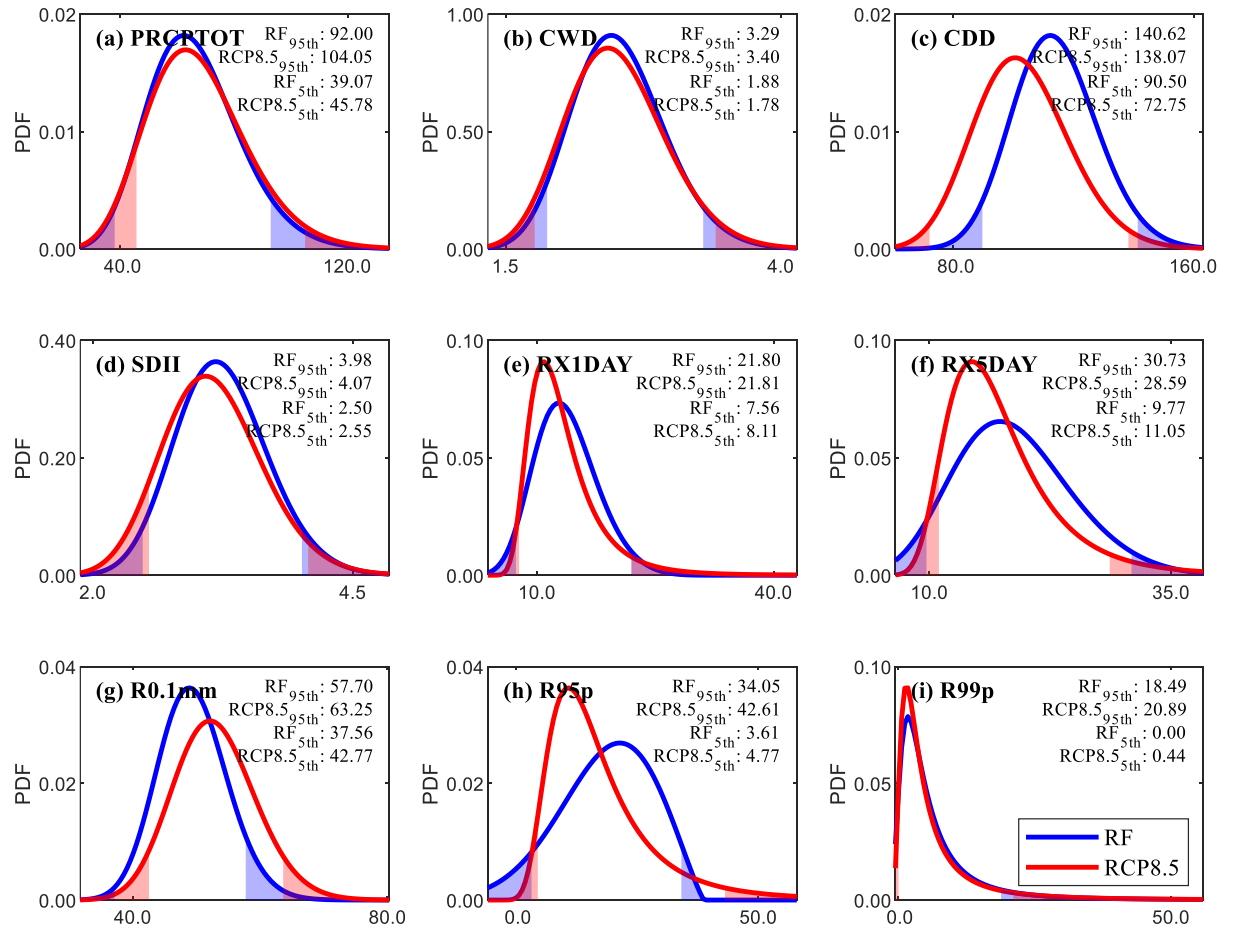


Figure S4. Annual probability density function (PDF) of the irrigation district averaged extreme precipitation indices from 1971 to 2000 (blue line, RF) and from 2021 to 2050 (red line, RCP8.5)—consideration of portions exceeding the 95th percentile and below the 5th percentile.

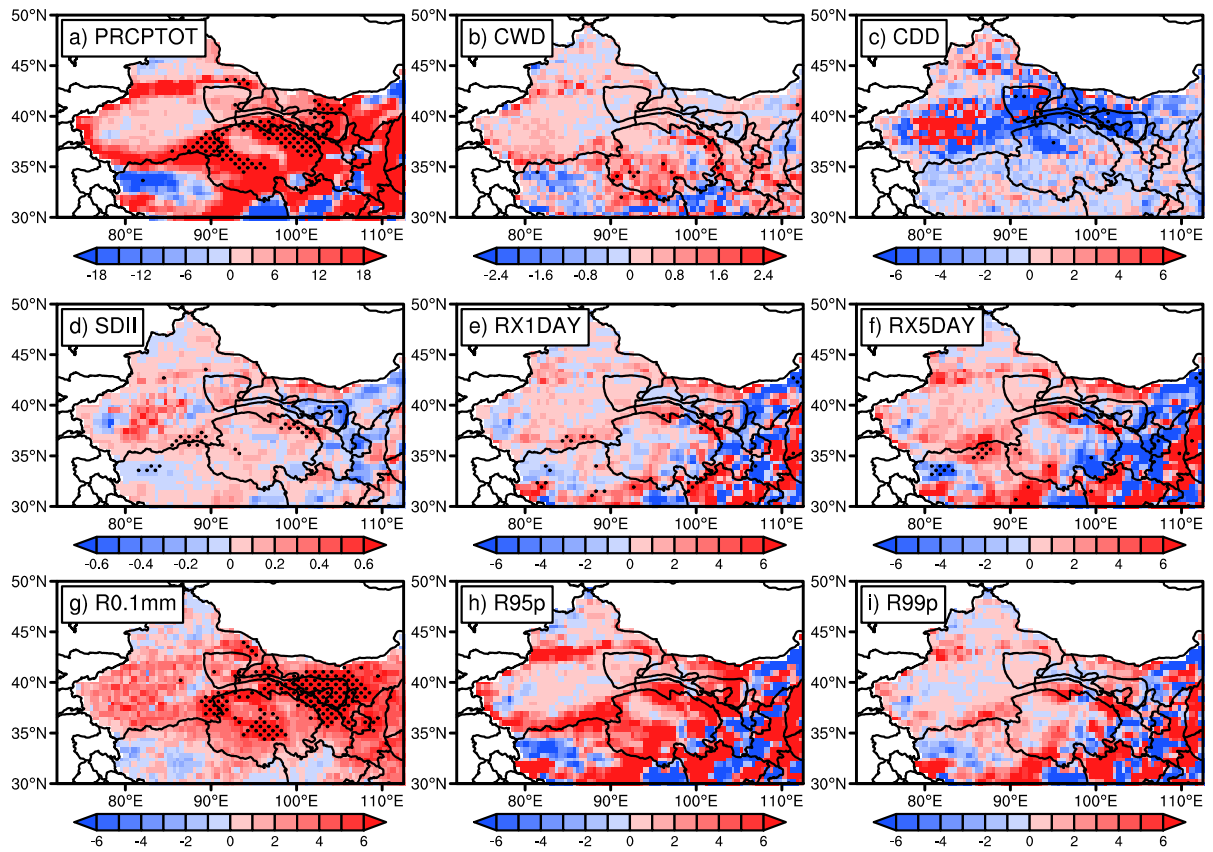


Figure S5. Multiyear average changes of extreme precipitation indices with and without irrigation under the RCP4.5 (defined as with-irrigation minus without-irrigation). The black dots represent statistically significant differences at the 95% significance level based on Student's t-test.

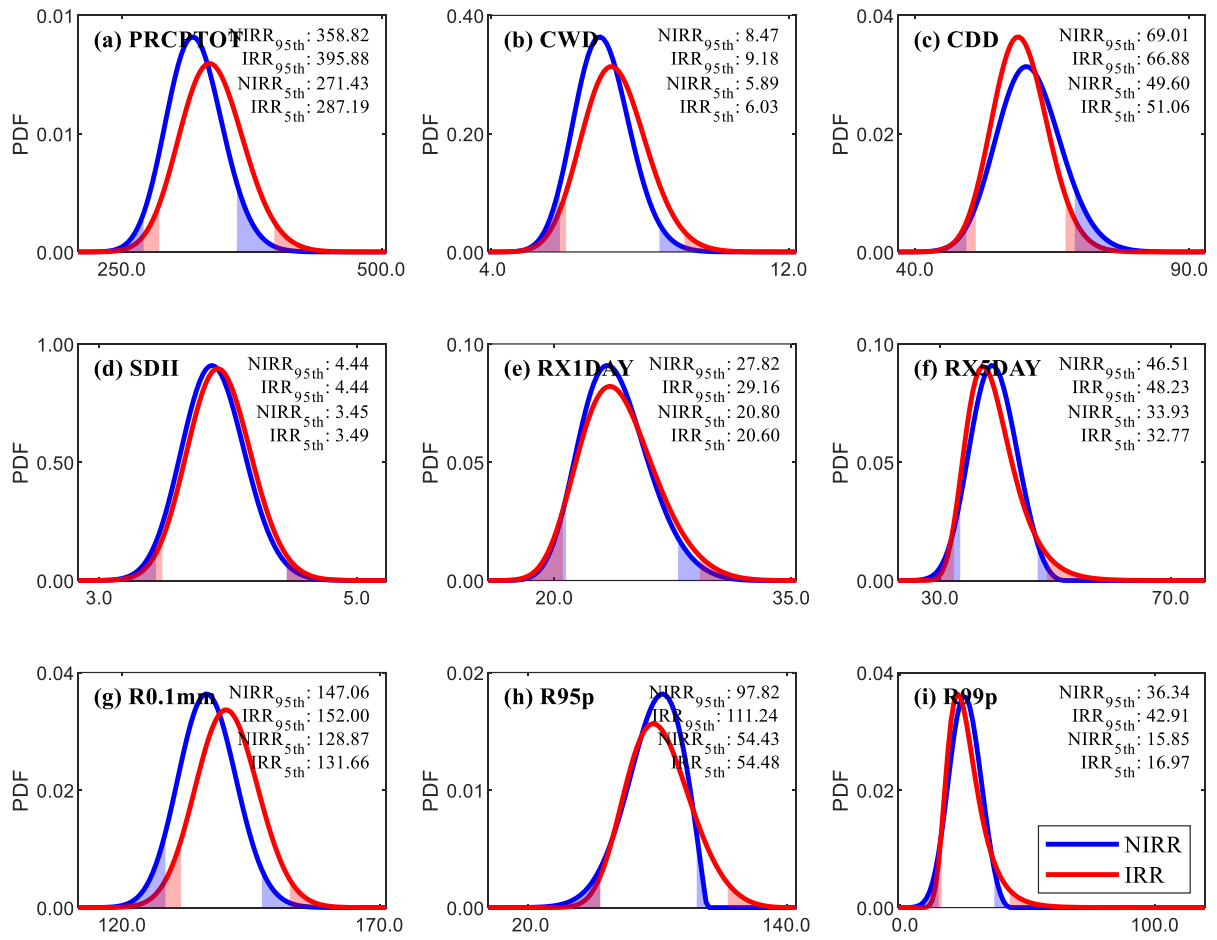


Figure S6. Annual probability density function (PDF) of Northwest China averaged extreme precipitation with (red line, IRR) and without (blue line, NIRR) irrigation under the RCP4.5—consideration of portions exceeding the 95th percentile and below the 5th percentile.

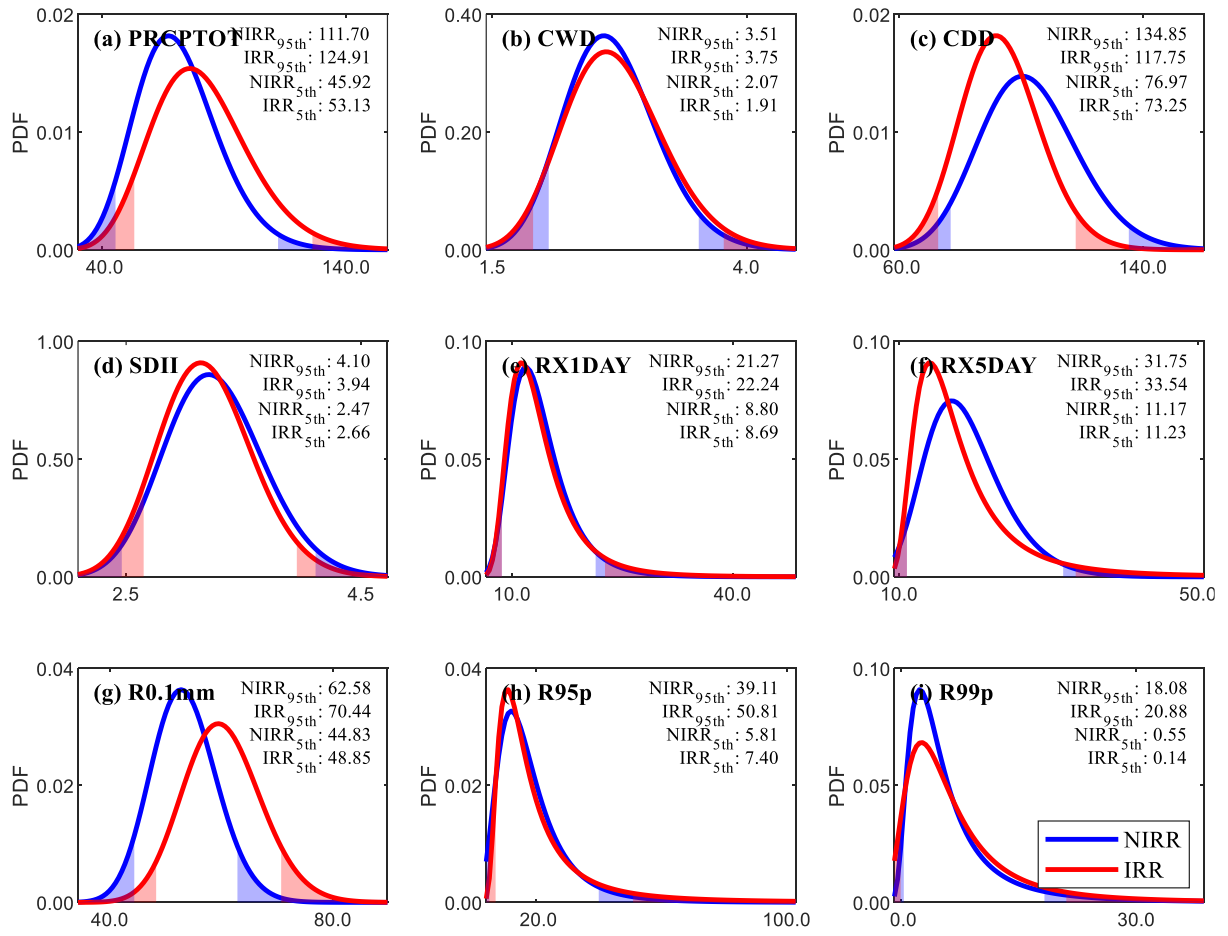


Figure S7. Annual probability density function (PDF) of the irrigation district averaged extreme precipitation with (red line, IRR) and without (blue line, NIRR) irrigation under the RCP4.5—consideration of portions exceeding the 95th percentile and below the 5th percentile.

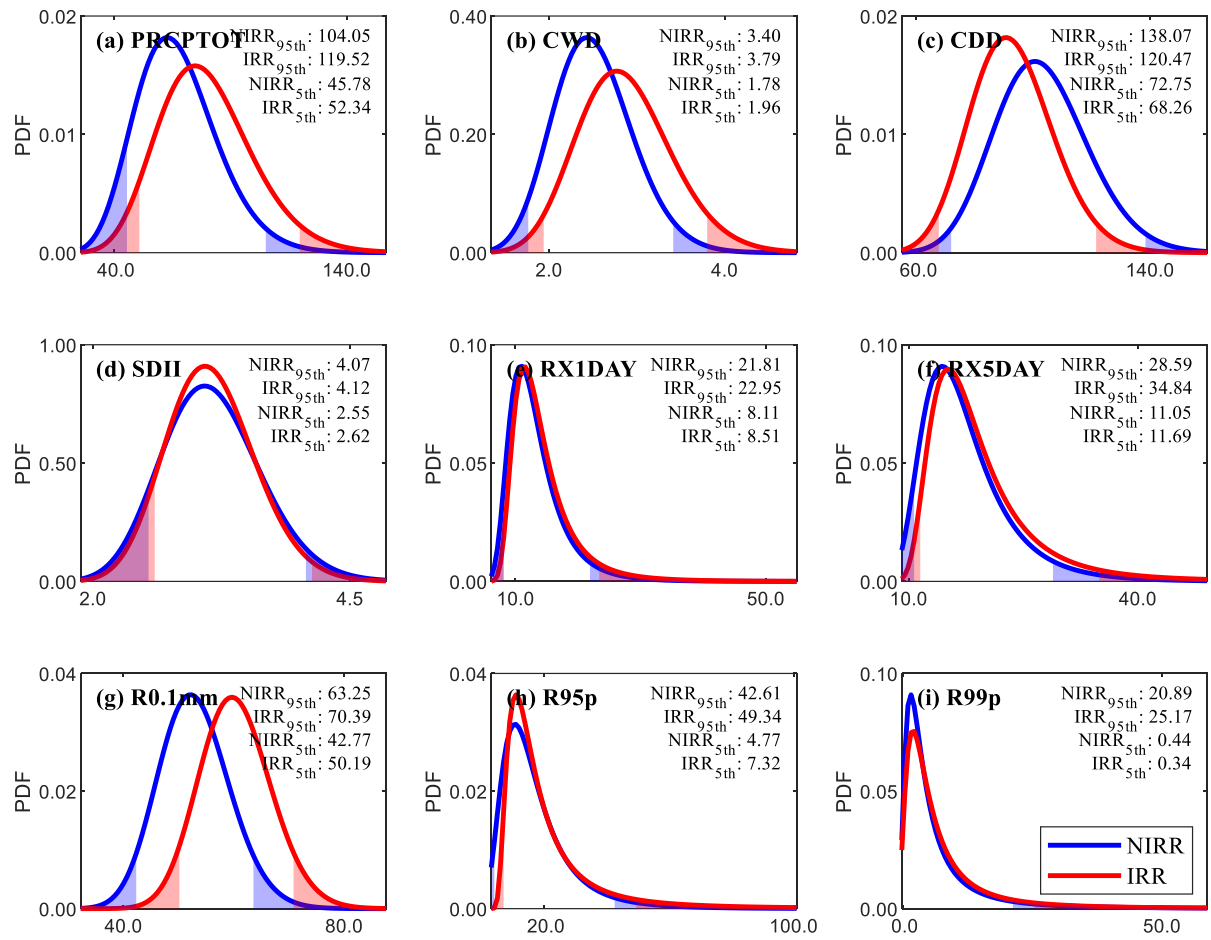


Figure S8. Annual probability density function (PDF) of the irrigation district averaged extreme precipitation with (red line, IRR) and without (blue line, NIRR) irrigation under the RCP8.5—consideration of portions exceeding the 95th percentile and below the 5th percentile.

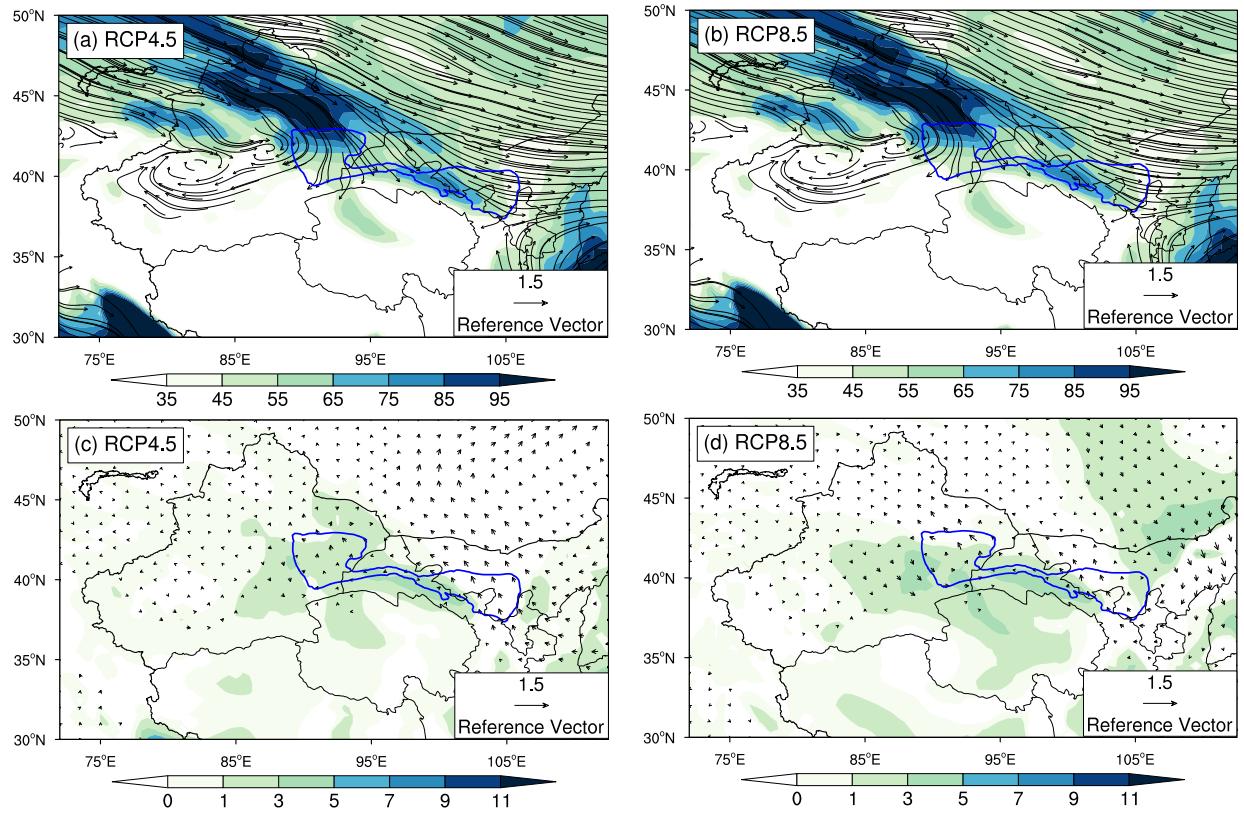


Figure S9. Upper panels: Summer climatology (2021-2050) of vertically integrated water vapor transport (shaded, $\text{kg}\cdot\text{m}^{-1}\cdot\text{s}^{-1}$) and low-level circulation (arrows, $\text{m}\cdot\text{s}^{-1}$) at 700 hPa for two different scenarios: a) RCP4.5, and b) RCP8.5. Bottom panels: Difference in the distribution of vertically integrated water vapor transport (shaded, $\text{kg}\cdot\text{m}^{-1}\cdot\text{s}^{-1}$) and low-level circulation (arrows, $\text{m}\cdot\text{s}^{-1}$) at 700 hPa between irrigated and non-irrigated for scenarios: c) RCP4.5, and d) RCP8.5. Blank areas represent regions with elevations exceeding 3000 meters.

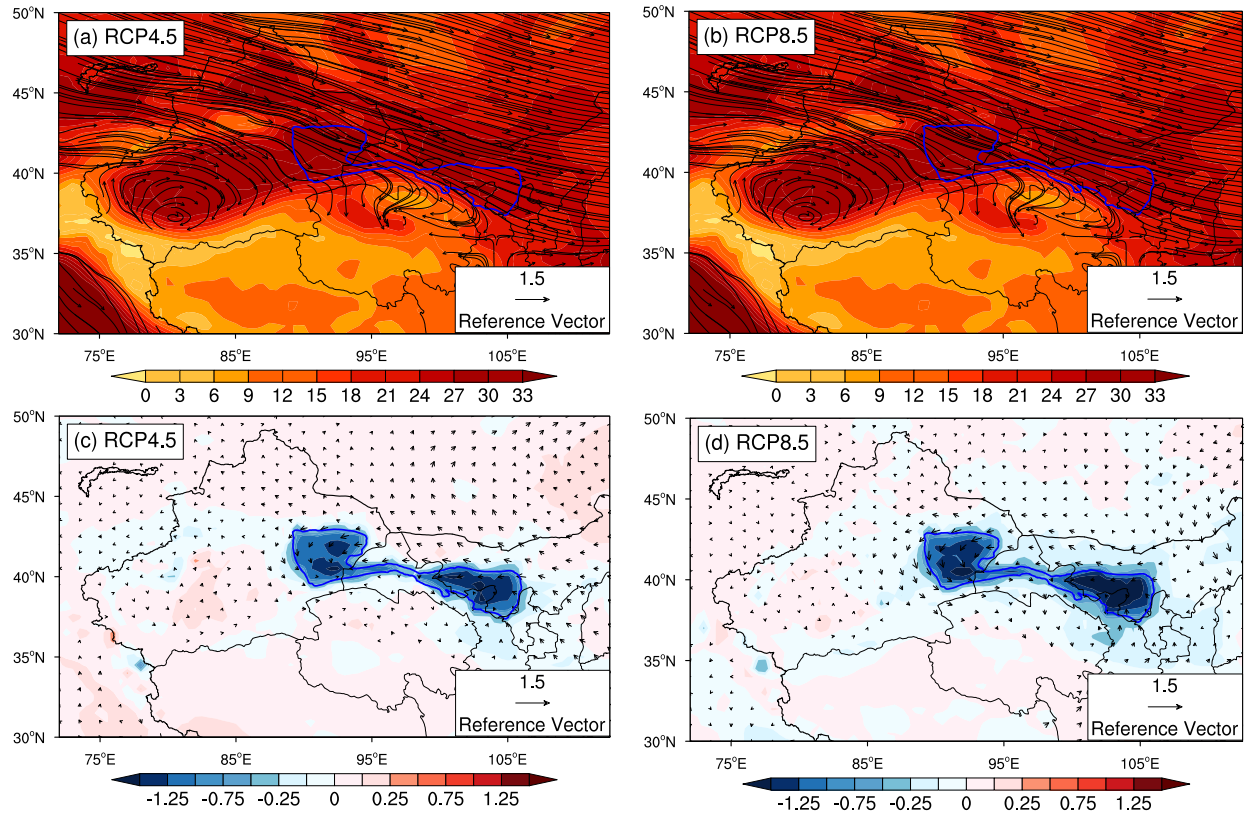


Figure S10. Upper panels: Summer climatology (2021-2050) of vertically integrated temperature (shaded, °C) and low-level circulation (arrows, $\text{m}\cdot\text{s}^{-1}$) at 600 hPa for two different scenarios: a) RCP4.5, and b) RCP8.5. Bottom panels: Difference in the distribution of vertically integrated temperature (shaded, °C) and low-level circulation (arrows, $\text{m}\cdot\text{s}^{-1}$) at 600 hPa between irrigated and non-irrigated for scenarios: c) RCP4.5, and d) RCP8.5. Blank areas represent regions with elevations exceeding 3000 meters.

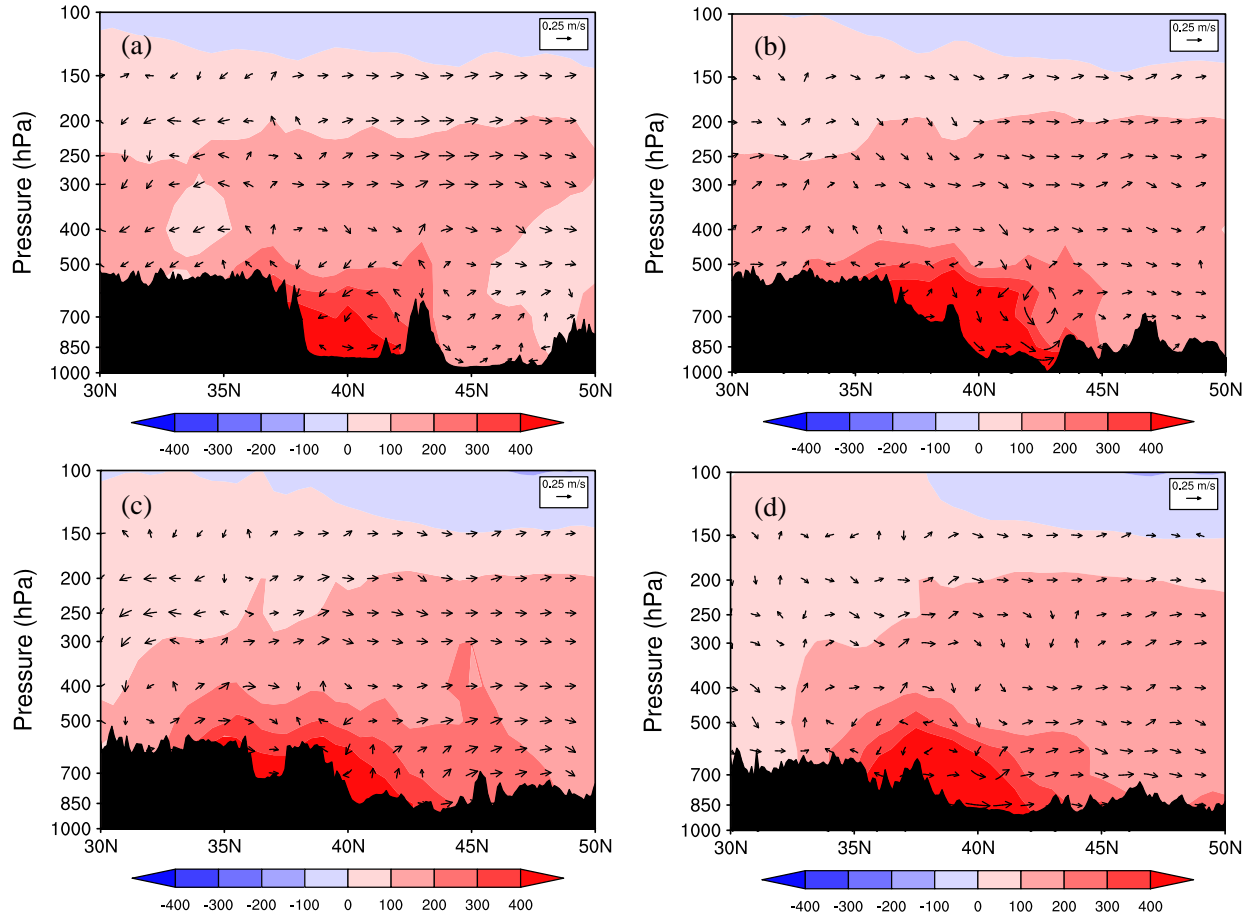


Figure S11. Vertical cross-section as a function of latitude for the difference (defined as with-irrigation minus without-irrigation) of summer meridional circulations (arrows; unit: $\text{m}\cdot\text{s}^{-1}$) and MSE (shaded; unit: $\text{J}\cdot\text{kg}^{-1}$) under the RCP4.5. (a~d are the vertical cross-section of 87°E , 92°E , 97°E , and 102°E , respectively. The black-shaded areas indicate the topography. The vertical component of wind velocity is exaggerated by a factor of 100.)